Physics of frequency-modulated comb generation in quantum-well diode lasers

Mark Dong,[1,2,*] Steven T. Cundiff,[1,2,†] and Herbert G. Winful[1,‡]

[1]*Department of Electrical Engineering and Computer Science, University of Michigan, 1301 Beal Avenue, Ann Arbor, Michigan 48109-2122, USA*

[2]*Department of Physics, University of Michigan, 450 Church Street, Ann Arbor, Michigan 48109-1040, USA*

We investigate the physical origin of frequency-modulated combs generated from single-section semiconductor diode lasers based on quantum wells, isolating the essential physics necessary for comb generation. We find that the two effects necessary for comb generation—spatial hole burning (leading to multimode operation) and four-wave mixing (leading to phase locking)—are indeed present in some quantum-well systems. The physics of comb generation in quantum wells is similar to that in quantum dot and quantum cascade lasers. We discuss the nature of the spectral phase and some important material parameters of these diode lasers.

I. INTRODUCTION

Optical frequency combs consist of discrete, narrow, equally spaced spectral lines that have a fixed phase relationship between them. These combs can span a frequency range that exceeds an octave in some cases and have found important applications in areas such as metrology, spectroscopy, and optical communications [1–4]. Methods for generating frequency combs include the mode locking of bulk lasers such as Ti:sapphire and fiber lasers and the nonlinear process of four-wave mixing in microresonators. These methods result in periodic trains of short pulses in the time domain whose Fourier transform corresponds to a frequency-comb spectrum. Another approach that has attracted recent interest is the direct generation of frequency combs from semiconductor lasers through a spontaneous phase-locking process that yields a frequency-modulated (FM) but continuous-wave (cw) or quasi-cw output. The cw operation avoids the detrimental phase effects of intracavity high-intensity pulse propagation [5], while the semiconductor platform offers the possibility of a portable, chip-scale device with low power consumption. FM combs have been experimentally demonstrated in quantum well- (QW) [6,7], quantum dot- (QD), and quantum dash (QDash) lasers [8,9], as well as in quantum cascade lasers (QCLs) [10]. While there have been theoretical explanations for FM-comb generation in QCLs [11] and in QD lasers [12,13], the physics of FM-comb generation in QW systems has been largely unexplored.

The formation of passively mode-locked FM combs in QD lasers and QCLs has been attributed to a variety of physical effects. Models of QD and quantum dash lasers had shown the importance of longitudinal spatial hole burning (SHB), treated as a gain compression term [12], or as a carrier grating term [13] which gives rise to multimode operation.

The large inhomogeneous gain broadening provided by the QD gain medium requires great effort to properly model the inhomogeneous distribution of quantum dots. Additional physical effects have also been proposed as important in affecting comb generation in QD lasers, including four-wave mixing (FWM), Kerr nonlinearities, and group velocity dispersion (GVD) [14–16]. Both FWM and Kerr nonlinearities are important to the locking of phases, while minimal GVD is typically desirable for phase locking especially at large bandwidths. For QCLs, the effect of the short upper-state population lifetime for intraband transitions has been the focus [12,16]. The short gain recovery in QCLs has been identified as a mechanism that naturally favors the FM mode-locked state as opposed to the traditional mode locking that generates a pulse train. Despite the plethora of effects that have been investigated in other systems, all of which can contribute to the generation of FM combs, there is still a need to clarify the essential mechanisms that allow some single-section diode lasers to produce such phase-locked combs without a saturable absorber.

Our goal is to explore and elucidate the essential physical effects for the generation of FM combs in QW diode lasers, showing that FM-comb generation from QW systems is certainly possible for certain material parameters. We find only two requirements for FM-comb generation: a mechanism for phase locking, which is fulfilled by FWM facilitated by population pulsations [17], and a mechanism for multimode generation, which is fulfilled by SHB due to standing-wave effects in the laser cavity that gives rise to multimode lasing. This conclusion may be surprising, as previous papers have argued that SHB can be ignored in QW lasers due to the long diffusion length ($\sim 2-3 \, \mu$m) relative to the wavelength, smearing out the spatial carrier grating [17–19]. We find that in the case of a free-running Fabry-Perot laser operating under a quasi-cw state, the carrier lifetime is significantly shortened due to the continuous presence of stimulated emission [20]. Such a difference not only improves FWM, but greatly reduces the diffusion length and allows SHB to occur.

*markdong@umich.edu
†cundiff@umich.edu
‡arrays@umich.edu

II. BACKGROUND

The realization that FWM and SHB are present in interband laser diodes is not new. There have been many experimental and theoretical papers investigating FWM in bulk and QW semiconductor optical amplifiers (SOAs) and lasers [17,21–23]. In particular, significant FWM efficiency in SOAs even up to detunings of 10 nm or about 1 THz at the 1550-nm operating point has been shown [23]. This detuning is much larger than the normal free spectral range of a typical semiconductor diode laser, which has longitudinal mode spacing of 10–100 GHz. This result suggests that FWM should be significant in QW lasers. Indeed, it has been shown that FWM is responsible for the passive mode locking that leads to self-pulsations in QW-distributed Bragg reflector lasers [24]. On the other hand, SHB has been clearly linked to multimode operation [25,26]. In QW lasers, both of these effects can be strong given the right parameters, leading to a FM mode-locked state.

We begin our investigation from a set of simplified equations [Eqs. (1) and (2)], derived from the Maxwell-Bloch equations. They consist of a single carrier population equation, a population grating equation, and a multimode electric-field equation. These equations resemble the higher-order equations in Chow *et al.* [27], in which the polarization has been adiabatically eliminated. This approach allows for a more accurate theory than the third-order perturbation approach while simultaneously reducing the number of equations to solve. The resulting equations are

$$
\frac{\partial \rho_{\mathrm{qw}}}{\partial t} = \frac{\eta I_{\mathrm{in}}}{q N_{\mathrm{qw}}}(1 - \rho_{\mathrm{qw}}) - \frac{\rho_{\mathrm{qw}}}{\tau_{\mathrm{sp}}}
$$
$$
- R(2\rho_{\mathrm{qw}} - 1)\mathrm{Re}(E_+^* F_+ + E_-^* F_-) \tag{1a}
$$

$$
\frac{\partial \rho_g}{\partial t} = -\frac{\rho_g}{\tau_{\mathrm{sp}}} - 4k_0^2 D\rho_g - R\left[\frac{1}{2}(E_+^* F_- + F_+^* E_-)(2\rho_{\mathrm{qw}}-1)\right.
$$
$$
\left. + 2\mathrm{Re}(E_+^* F_+ + E_-^* F_-)\rho_g\right] \tag{1b}
$$

$$
\pm\frac{\partial E_\pm}{\partial z} + \frac{1}{v_g}\frac{\partial E_\pm}{\partial t}
$$
$$
= -\frac{\alpha}{2}E_\pm + \frac{g}{2}\left[(2\rho_{\mathrm{qw}} - 1)F_\pm + 2\rho_g^{(*)}F_\mp\right] + S_{\mathrm{sp}}, \tag{2}
$$

where ρ_{qw} is the quantum-well carrier population, ρ_g is the population grating amplitude, η is the quantum efficiency, I_{in} is the input current, N_{qw} is the effective, reduced 2D number of electron and hole states available, τ_{sp} is the spontaneous emission lifetime, S_{sp} is spontaneous emission noise, D is the ambipolar diffusion coefficient, $R = 2gL/\hbar\omega_0 N_{\mathrm{qw}}$ is the recombination factor, L is the length of the device, and ω_0 is the transition frequency. N_{qw} is related to the traditional joint 2D density of states, $N_{\mathrm{qw}} = D_r^{2D} V_{\mathrm{eff}}\hbar\Gamma$, where $V_{\mathrm{eff}} = h_{\mathrm{qw}} W L$ is the total effective volume of the QW, and Γ is the homogenous linewidth. The filtered field variable,

$$
F_\pm = \Gamma\int_{-\infty}^{t} dt' e^{-\Gamma(t-t')}E_\pm(z,t'), \tag{3}
$$

is derived from assuming the microscopic polarization decoheres fast enough to adiabatically follow the electric fields, which results in a Lorentzian distribution of the gain profile

with half linewidth Γ. This convenient way to write the multimode electric field avoids introducing additional envelope variables and is easily numerically calculated.

These equations contain the physical effects of FWM via population pulsations in ρ_{qw} (driven by the beating between field components) and the physical effects of SHB via the presence of ρ_g. It is important to note that, while other physical effects including chromatic and waveguide dispersion, Kerr nonlinearities, and inhomogeneous gain broadening are certainly important and can greatly affect comb performance, we discard them here to show that they are not essential for comb formation. In fact, these effects often inhibit comb formation, but because we have already demonstrated the viability of comb generation with these effects included [28], our goal here is to focus on the reduced model and extract some physical understanding.

We first apply a simplified analytic approach to Eqs. (1) and (2) and perform a perturbation analysis on the behavior of the side modes of the laser. Then, to verify our analytic results, we solve Eqs. (1) and (2) numerically for two material systems, GaAs QWs and InGaAsP QWs, each with a different central lasing wavelength and diffusion coefficient. We pay specific attention to the effects of carrier grating terms responsible for SHB in these solutions.

III. PERTURBATION ANALYSIS

We take a closer look at the important physics behind the system by applying a perturbative approach to Eqs. (1) and (2), showing specifically where FWM and SHB are significant and how they affect laser operation. Our approach is to first assume steady-state, single-mode operation for the laser, and then look at the evolution of the side-bands as a perturbative effect. The amplitude stability of the sideband modes indicates whether the laser tends to multimode operation, while the phase evolution indicates if, and how, the modes lock together. The initial assumption of single-mode operation may seem restrictive, and certainly the results are less applicable once the laser assumes multimode operation, but because we are looking at the stability of the side modes, much understanding can still be gained on the conditions in which the laser deviates from single mode.

A. Single-mode operation

We write the electric-field and carrier population equations for single-mode operation as is typically done for interband semiconductor lasers. We ignore the carrier grating term and carrier pulsations for now, but will include them again later in our multimode analysis. The electric-field and population variables simplify to $E_+ \to A_0, E_- \to B_0, \rho_{\mathrm{qw}} \to \rho_0$. Under this assumption, the filtered field is $F_\pm = A_0, B_0$. The steady-state solution for the population is

$$
\rho_0 = \tau_{\mathrm{cw}}\frac{\eta I_{\mathrm{in}}}{q N_{\mathrm{qw}}} + \tau_{\mathrm{cw}}R(|A_0|^2 + |B_0|^2), \tag{4}
$$

where

$$
\tau_{\mathrm{cw}} = \left[\frac{\eta I_{\mathrm{in}}}{q N_{\mathrm{qw}}} + \frac{1}{\tau_{\mathrm{sp}}} + 2R(|A_0|^2 + |B_0|^2)\right]^{-1}. \tag{5}
$$

Using Eq. (4) in Eq. (2), we obtain the equations for the steady-state electric field

$$\frac{dA_0}{dz} = -\frac{\alpha}{2}A_0 + \frac{g_{\mathrm{eff}}}{2}A_0, \quad -\frac{dB_0}{dz} = -\frac{\alpha}{2}B_0 + \frac{g_{\mathrm{eff}}}{2}B_0, \quad (6)$$

with total effective gain

$$g_{\mathrm{eff}} = g\left[2\tau_{\mathrm{cw}}\frac{\eta I_{\mathrm{in}}}{qN_{\mathrm{qw}}} + 2\tau_{\mathrm{cw}}R(|A_0|^2 + |B_0|^2) - 1\right]. \quad (7)$$

Despite the highly nonlinear nature of Eqs. (6) (especially due to τ_{cw}), we can obtain semianalytic solutions for the effective gain. We introduce an auxiliary variable $\theta(z)$, where $d\theta/dz = -\alpha/2 + g_{\mathrm{eff}}/2$ [29]. Substituting into Eqs. (6), we obtain much simpler equations with solutions

$$A_0 = C_1 \exp\left(-\frac{\alpha z}{2} + \frac{1}{2}\int_0^z dz' g_{\mathrm{eff}}\right),$$

$$B_0 = C_2 \exp\left(\frac{\alpha z}{2} - \frac{1}{2}\int_0^z dz' g_{\mathrm{eff}}\right).$$

We can apply the two reflective boundary conditions, $A_0(0) = \sqrt{r}B_0(0)$ and $B_0(L) = \sqrt{r}A_0(L)$, where r is the power reflection coefficient. These boundary conditions result in an expression for the effective gain in steady state

$$\frac{1}{L}\int_0^L dz g_{\mathrm{eff}} = \alpha + \frac{1}{2L}\ln(1/r^2) = g_{\mathrm{th}}. \quad (8)$$

The fact that the total integrated gain (or simply gain if it is a constant) clamps to the threshold gain in steady state is a well-known feature of cw lasers. This fact is important in our subsequent stability analysis, as it suggests the sideband modes will have difficulty achieving threshold due to gain clamping.

B. Four-wave mixing

We now add in the physics of FWM and analyze the the growth, stability, and phase of the side modes. We introduce additional envelopes in the electric field, splitting it into individual components: the central mode and the nearest-neighbor cavity modes.

$$E_+ = A_{-1}e^{-i\omega_s t} + A_0 + A_1 e^{i\omega_s t}$$
$$E_- = B_{-1}e^{-i\omega_s t} + B_0 + B_1 e^{i\omega_s t}$$
$$\rho_{\mathrm{qw}} = \rho_0 + \rho_1 e^{i\omega_s t} + \rho_1^* e^{-i\omega_s t}. \quad (9)$$

The side-mode envelope amplitudes $A_{\pm 1}, B_{\pm 1}$ are assumed to be small in the perturbation analysis such that we only keep terms that are linear in these quantities. However, the central mode A_0, B_0 is significant so we retain nonlinearities associated with them. The filtered field simplifies to $F_+ = c_s^* A_{-1}e^{-i\omega_s t} + A_0 + c_s A_1 e^{i\omega_s t}$. The constant $c_s = 1/(1 + i\omega_s/\Gamma)$ is a filtering term that adjusts for the gain away from the center of the Lorentzian and $|c_s| < 1$. After inserting

Eqs. (9) into Eq. (1a) we solve for the carrier population

$$\rho_1 = -R\tau_p(2\rho_0 - 1)\frac{c_s + 1}{2}(A_0^* A_1 + A_0 A_{-1}^*$$
$$+ B_0^* B_1 + B_0 B_{-1}^*), \quad (10)$$

$$\tau_p = \left[\frac{1}{\tau_{\mathrm{sp}}} + i\omega_s + 2R(|A_0|^2 + |B_0|^2)\right]^{-1}. \quad (11)$$

Here, we emphasize that in a laser operating quasi-cw, both the static and pulsating carrier lifetimes, given by τ_{cw} and τ_p, respectively, are shortened by the presence of light inside the cavity due to stimulated emission. We want to distinguish, however, that while the absolute value of the pulsating carrier lifetime $|\tau_p|$ decreases, the real part, or in-phase component of the carrier population, greatly increases relative to the imaginary part, or quadrature component of the carrier population. This effect is seen in the lifetime dependence upon the total intracavity power, $P_0 = |A_0|^2 + |B_0|^2$. For even modest values of intracavity power such as $P_0 \approx 8\,\mathrm{mW}$, the cw carrier lifetime decreases from a few ns to the order of a few ps, while the proportion of the real part of the pulsating carrier lifetime exceeds 50%, allowing for the oscillating population to follow the dynamics caused by adjacent cavity modes. Thus, despite a long spontaneous emission lifetime, the above lifetimes are modified enough via stimulated emission to allow FWM to occur. Using Eq. (10) in Eq. (2) gives the individual mode equations

$$\frac{dA_1}{dz} = -\frac{\alpha}{2}A_1 + \frac{g_{\mathrm{eff}}}{2}c_s A_1 - g_2\big(|A_0|^2 A_1$$
$$+ A_0^2 A_{-1}^* + A_0 B_0^* B_1 e^{2i\Delta k} + A_0 B_0 B_{-1}^* e^{2i\Delta k}\big)$$

$$\frac{dA_{-1}}{dz} = -\frac{\alpha}{2}A_{-1} + \frac{g_{\mathrm{eff}}}{2}c_s^* A_{-1} - g_2^*\big(|A_0|^2 A_{-1} + A_0^2 A_1^*$$
$$+ B_0 A_0 B_1^* e^{-2i\Delta k} + B_0^* A_0 B_{-1} e^{-2i\Delta k}\big)$$

$$-\frac{dB_1}{dz} = -\frac{\alpha}{2}B_1 + \frac{g_{\mathrm{eff}}}{2}c_s B_1 - g_2\big(|B_0|^2 B_1 + B_0^2 B_{-1}^*$$
$$+ B_0 A_0^* A_1 e^{2i\Delta k} + B_0 A_0 A_{-1}^* e^{-2i\Delta k}\big)$$

$$-\frac{dB_{-1}}{dz} = -\frac{\alpha}{2}B_{-1} + \frac{g_{\mathrm{eff}}}{2}c_s^* B_{-1} - g_2^*\big(|B_0|^2 B_{-1} + B_0^2 B_1^*$$
$$+ B_0 A_0 A_1^* e^{2i\Delta k} + B_0 A_0^* A_{-1} e^{2i\Delta k}\big), \quad (12)$$

where gain saturation, $g_2 = gR(2\rho_0 - 1)\tau_p(c_s + 1)/2$, exists due to the presence of population pulsations ρ_1. This term is physically responsible for additional self-saturation [the first term in the brackets in Eqs. (12)] as well as FWM with the other modes. The spatial-phase-mismatch term $\Delta k = \omega_s/v_g$ (where $\omega_s/2\pi$ is the free spectral range) originates from the frequency difference between cavity modes.

Equations (12) can be solved analytically given the following assumptions. First, we neglect the phase-mismatched terms and decouple the forward and backward waves. Next, the homogeneous linewidth 2Γ (on the order of 1 THz) should be much broader than the free spectral range $\omega_s/2\pi$ (tens of GHz), meaning $c_s \approx 1$. Lastly, because of the clamping of the effective gain as discussed in the previous section, we eliminate the gain and loss terms in Eq. (12) due to no net

gain or loss in a round trip. Making these approximations, and rewriting $A_0 = |A_0|e^{i\psi_0}$, we obtain coupled equations for the forward-propagating modes

$$\frac{dA_1}{dz} = -g_2|A_0|^2(A_1 + A_{-1}^* e^{2i\psi_0})$$

$$\frac{dA_{-1}^*}{dz} = -g_2|A_0|^2(A_{-1}^* + A_1 e^{-2i\psi_0}). \qquad (13)$$

Again, we can solve these by introducing the auxiliary variable $\theta(z)$, but with $d\theta/dz = g_2|A_0|^2$ and solving the equations with respect to $\theta(z)$. We note that ψ_0, the phase of the cw envelope, is independent of z. Equations (13) reduce to a 2×2 eigenvalue problem

$$\frac{d}{d\theta}\begin{bmatrix} A_1 \\ A_{-1}^* \end{bmatrix} = -\begin{bmatrix} 1 & e^{2i\psi_0} \\ e^{-2i\psi_0} & 1 \end{bmatrix}\begin{bmatrix} A_1 \\ A_{-1}^* \end{bmatrix}. \qquad (14)$$

The solutions to Equation (14) consist of the eigenvalues $\lambda_1 = 0, \lambda_2 = -2$ and the general solution for the side modes is

$$\begin{bmatrix} A_1 \\ A_{-1}^* \end{bmatrix} = C_1\begin{bmatrix} -e^{2i\psi_0} \\ 1 \end{bmatrix}$$

$$+ C_2 \exp\left(-2\int_0^z dz' g_2|A_0|^2\right)\begin{bmatrix} e^{2i\psi_0} \\ 1 \end{bmatrix}. \quad (15)$$

These solutions show that it is not possible for either side mode A_1 or A_{-1} to grow in amplitude through FWM. This conclusion is supported by the fact that the integral in the exponential is always positive and that neither eigenvalue has a positive real part. Simply increasing the strength of FWM by increasing g_2 will not lead to multimode operation, as it simultaneously increases the self-saturation due to the population pulsations.

Our major conclusion is that, in QW diode lasers, FWM can certainly exist and lock phases together due to the modified carrier lifetime τ_p but is not strong enough to sustain additional modes against gain competition. The combination of the overall gain being clamped at threshold by self-saturation due to population pulsations greatly limits the ability of FWM to generate additional modes, thus masking the existence of FWM. So, the second requirement for comb generation, a mechanism for multimode lasing, remains unfulfilled. This situation is in stark contrast to FWM in Kerr combs, which use a very strong external pump laser [30] able to provide the power necessary to sustain the modes. The same effect is also present in FWM experiments in SOAs in which external lasers (cw or pulsed) are used. In addition, some FWM experiments can have lower power inputs that only weakly saturate the gain as opposed to strong saturation in a free-running laser. The weak saturation allows the sideband modes to achieve gain [23].

C. Spatial hole burning

Having shown that FWM alone is insufficient to result in multimode lasing, we add the effect of the carrier grating in order to include SHB. We assume the population grating has only a single component as only the strong central mode should contribute to any significant carrier grating in the perturbation approximation, $\rho_g \to \rho_{g0}$ From Eq. (1b), we find the

steady-state solution,

$$\rho_{g0} = -R(2\rho_0 - 1)\tau_g B_0 A_0^*, \qquad (16)$$

$$\tau_g = \left[\frac{1}{\tau_{sp}} + 4k_0^2 D + 2R(|A_0|^2 + |B_0|^2)\right]^{-1}. \quad (17)$$

Use of Eq. (16) in the single-mode electric-field equations modifies Eqs. (6) to have an additional self-saturation term due to the population grating

$$\frac{dA_0}{dz} = -\frac{\alpha}{2}A_0 + \frac{g_{eff}}{2}A_0 - gR(2\rho_0 - 1)\tau_g|B_0|^2 A_0$$

$$-\frac{dB_0}{dz} = -\frac{\alpha}{2}B_0 + \frac{g_{eff}}{2}B_0 - gR(2\rho_0 - 1)\tau_g|A_0|^2 B_0. \qquad (18)$$

The presence of the additional loss from the carrier grating affects the steady-state value of the gain and the intracavity fields. Now, g_{eff} is no longer clamped to the threshold gain. Using the same methods as before, we derive the new expression for the effective gain under SHB,

$$\frac{1}{L}\int_0^L dz g_{eff} = g_{th} + \frac{2}{L}\int_0^L dz g_3|B_0|^2, \qquad (19)$$

where $g_3 = gR(2\rho_0 - 1)\tau_g$ is a measure of the strength of the carrier grating. Using this new expression for g_{eff} in Eqs. (12) and making the same approximations as the preceding section, we obtain the modified FWM equations

$$\frac{dA_1}{dz} = (g_3|B_0|^2 - g_2|A_0|^2)A_1 - g_2|A_0|^2 A_{-1}^* e^{2i\psi_0}$$

$$\frac{dA_{-1}^*}{dz} = (g_3|B_0|^2 - g_2|A_0|^2)A_{-1}^* - g_2|A_0|^2 A_1 e^{-2i\psi_0}, \quad (20)$$

where additional gain is available by approximately the strength of the SHB term. The general solutions to Eqs. (20) are

$$\begin{bmatrix} A_1 \\ A_{-1}^* \end{bmatrix} = C_1 \exp\left(\int_0^z dz' g_3|B_0|^2\right)\begin{bmatrix} -e^{2i\psi_0} \\ 1 \end{bmatrix}$$

$$+ C_2 \exp\left(\int_0^z dz'(g_3|B_0|^2 - 2g_2|A_0|^2)\right)\begin{bmatrix} e^{2i\psi_0} \\ 1 \end{bmatrix}, \qquad (21)$$

which are similar to solutions in Eqs. (15), albeit with the eigenvalues shifted by the availability of additional gain. In this form, both forward waves have the potential to grow exponentially now that the integrals in the exponentials can be positive. From Eq. (21), there is no concrete cutoff for the minimum value of g_3, but the gain of the side modes is a continuum depending upon the intracavity power and length of the cavity. However, it is preferable for g_3, or τ_g, to be large such that the additional gain over the cavity length L is appreciable for strong growth of the sidebands relative to the center mode. In other words, the grating must be sufficiently strong, or equivalently, the grating lifetime must be sufficiently large, such that the gain competition is weakened due to unused gain now available inside the cavity.

Our conclusion is that SHB is indeed present in some QW systems, with the major criteria being a low diffusion coeficient

and a long operating wavelength. SHB reduces the effects of gain competition and increases the total gain seen by the side modes. It is primarily this SHB effect, not FWM, that induces multimode lasing. In other laser systems, the SHB requirement is easily fulfilled: A long operating wavelength in QCLs greatly reduces the ability of diffusion to wash out the spatial holes, while negligible diffusion in QD lasers allows for even gratings with very short spacings to survive. Once the system is in multimode operation, FWM takes over to lock the phases of these modes together.

D. Phase-locked solutions

Now that we have established the physical mechanism for how the modes emerge, we take a closer look at how the phases are locked together and why they tend to a FM solution rather than a pulse train. Rewriting Eqs. (20) in terms of magnitude and phase components $A_1 = |A_1|e^{i\psi_1}, A_{-1} = |A_{-1}|e^{i\psi_{-1}}$ gives

$$\frac{d}{dz}|A_1| = (g_3|B_0|^2 - g_2|A_0|^2)|A_1|$$
$$- g_2|A_0|^2|A_{-1}|\cos(2\psi_0 - \psi_{-1} - \psi_1)$$

$$\frac{d}{dz}|A_{-1}| = (g_3|B_0|^2 - g_2|A_0|^2)|A_{-1}|$$
$$- g_2|A_0|^2|A_1|\cos(2\psi_0 - \psi_1 - \psi_{-1})$$

$$\frac{d}{dz}(\psi_1 + \psi_{-1}) = -g_2|A_0|^2 \sin(2\psi_0 - \psi_1 - \psi_{-1})$$
$$\times \left[\frac{|A_1|^2 + |A_{-1}|^2}{|A_1||A_{-1}|}\right]. \quad (22)$$

We assume for this analysis that g_2, and therefore τ_p, is approximately pure real, meaning we have a sizable amount of optical power inside the cavity. We see that the rate of phase evolution goes to zero when the argument of the sine becomes

$$\Phi = 2\psi_0 - \psi_1 - \psi_{-1} = \pm\pi, 0, \quad (23)$$

implying that these values of the phases indicate mode locking. However, a stability analysis shows that the zero solution is not stable. When $\psi_1 + \psi_{-1}$ increases, the derivative becomes $d/dz(\psi_1 + \psi_{-1}) \sim -\sin(0^-)$, which is positive and will grow away from $\Phi = 0$. We note that the zero phase-difference solution corresponds to a series of short pulses. Now, looking instead at the solution of $\Phi = \pm\pi$, which corresponds to a quasi-FM solution, this solution is stable. A physical interpretation of this stability can be as follows. At the $\Phi = \pm\pi$ phase configuration, the gain is maximized due to the way the fields interfere. If there is a slight shift in the phase of A_1, this in turn shifts the phase of the pulsating carrier population, which then tends to correct the phase of A^*_{-1} back toward the gain maximum.

The phase relation can be generalized to any mode n and summed to produce an expression for the phase ψ_{n+1} as a function of n [9]:

$$\sum_{m'=0}^{n}\sum_{m=0}^{m'} \Phi_m = \sum_{m'=0}^{n}\sum_{m=0}^{m'}(2\psi_m - \psi_{m+1} - \psi_{m-1}), \quad (24)$$

$$\psi_{n+1} = \frac{\pi n^2}{2} + \alpha n + \beta, \quad (25)$$

TABLE I. Parameters used in numerical simulations.

Parameter	Description	GaAs (InGaAsP) value
L	Length of device	500 μm
W	Width of waveguide	4 μm
h_{qw}	Height of quantum well	5 nm
n_0	Group refractive index	3.5
α	Intrinsic waveguide loss	5 cm^{-1}
$\hbar\omega_0$	Central transition energy	1.5 eV (0.8 eV)
Γ	Homogeneous half linewidth	4.0 meV/$\hbar$
g	Modal gain coefficient	50 cm^{-1}
N_{qw}	Effective number of QW states	2.34×10^6
τ_{sp}	Spontaneous emission lifetime	1 ns
ηI_{in}	Input current	30 mA
D	Ambipolar diffusion coefficient	20.0 cm^2/s (7.2 cm^2/s)

where α and β are arbitrary constants. The phase as a function of mode number n has a clear quadratic dependence, which can then be compensated via a simple dispersive medium to produce a series of short pulses. Moreover, at this value of Φ, the gain of the side modes $A_{\pm 1}$ also reaches a maximum. Thus, the FM solution emerges as the natural phase-locked solution in the presence of FWM and multimode lasing. This physically makes sense in light of gain competition. The various phases
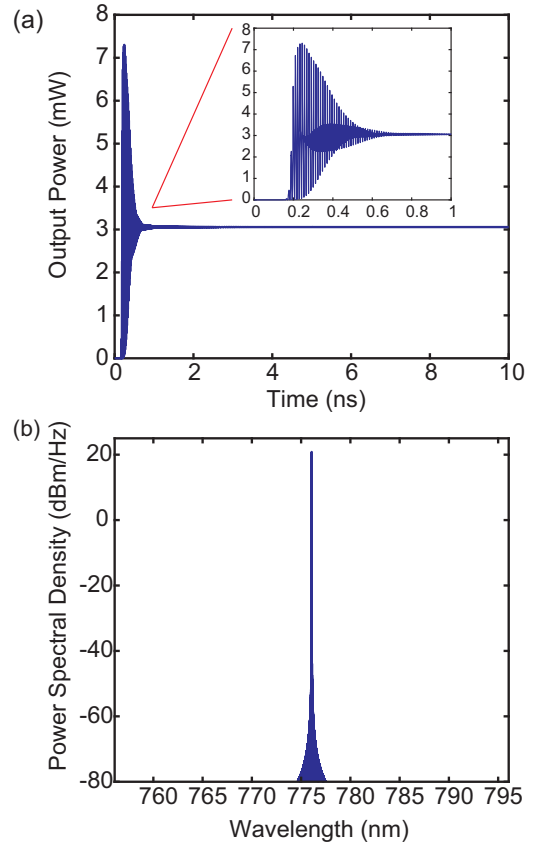

FIG. 1. Calculated output optical power for a diode laser with gain medium consisting of a GaAs quantum well. (a) Temporal power output, which settles down quickly to a single mode after the initial relaxation oscillations. (b) Spectrum of the temporal output showing a single mode.
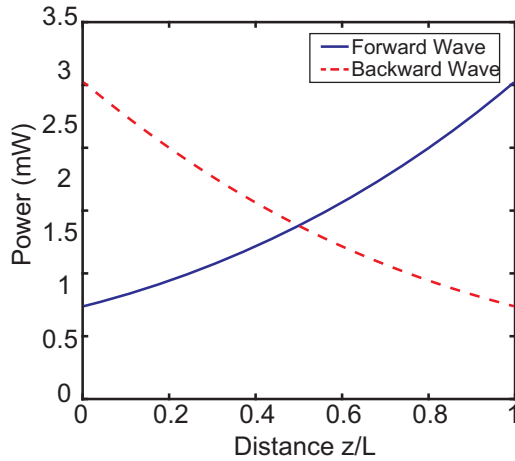
FIG. 2. Simulated steady-state optical power distribution inside the cavity for a GaAs quantum-well gain medium. The forward and backward waves are plotted, showing roughly symmetric, exponential solutions.

of the modes will settle to where the available gain is greatest, producing a natural phase offset between the different modes.

In other words, a solution in which all modes constructively add to form a train of pulses is not preferable (absent a saturable absorber) due to the inefficient use of the available gain in between pulses. Instead, the FM solution utilizes all available gain by having the modes interfere at different points in time, producing a stable, quasi-CW phase-locked state.

We are mindful that the above analysis has been performed under third-order perturbation in a single-mode state, so we expect the actual phases of the modes to deviate from Eq. (25) once the side modes become significant and the central mode is saturated. However, the general quadratic shape and FM nature are not lost, as confirmed by our numerical solutions in the following section.

IV. NUMERICAL SOLUTIONS

To illustrate the aforementioned ideas, we numerically solve the traveling-wave equations coupled with the carrier rate equations [Eqs. (1) and (2)] via a first-order Euler method along characteristics. We solve the equations for two sets of parameters for the gain medium corresponding to a GaAs QW or an InGaAsP QW, as given in Table I. The major differences are a different central emission wavelength and
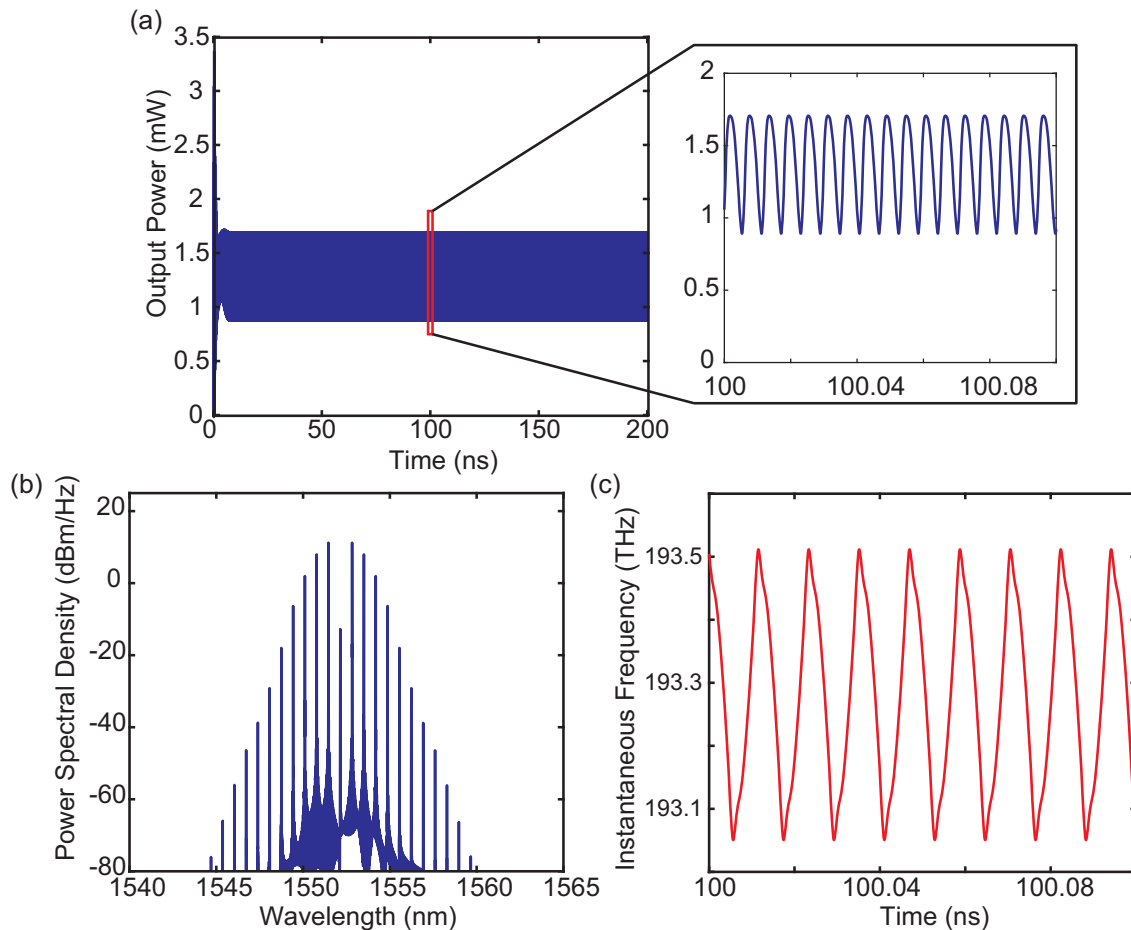

FIG. 3. Calculated output optical power for a diode laser with gain medium consisting of an InGaAsP quantum well. (a) Temporal power output with a zoomed-in inset at 100 ns is shown. (b) Spectrum of the InGaAsP quantum-well gain medium temporal output showing a frequency comb. (c) Instantaneous frequency of the output, plotted on the same timescale as the inset in (a), has a triangular, almost sawtoothlike profile when the phases are locked.
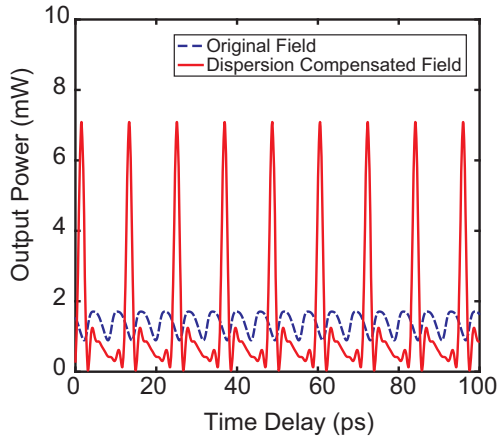
FIG. 4. Simulated temporal output from a diode laser with an InGaAsP quantum well for the gain medium after dispersion compensation. The spectrum from Fig. 3(b) is multiplied by quadratic phase to simulate dispersion compensation via an optical fiber. The group delay dispersion in this case is 1.1 ps².

a different diffusion coefficient. The results of this calculation for GaAs are shown in Figs. 1 and 2, and for InGaAsP shown in Figs. 3 and 4. The biggest contrast between the two results is that the GaAs calculation exhibits only a single mode, with the intracavity intensity profile shown in Fig. 2, while the InGaAsP calculation exhibits a comb which, in contrast with the solutions for GaAs quantum-well gain medium, does not settle to a single mode but eventually reaches a stable phase-locked state. This output can be dispersion compensated to form ultrashort pulses as shown in Fig. 4. The relative strength of the central comb lines in Fig. 3(b) has a remarkably similar shape to that of the spectrum obtained from experiment [31].

The determining criterion for coherent comb generation is whether or not SHB and FWM are significant inside the cavity. If the diffusion length is much smaller than the half wavelength, or in our model, if τ_g is large enough, then SHB will induce multimode lasing. Assuming a total intracavity power of $|A_0|^2 + |B_0|^2 \approx 5$ mW, the carrier lifetime and diffusion

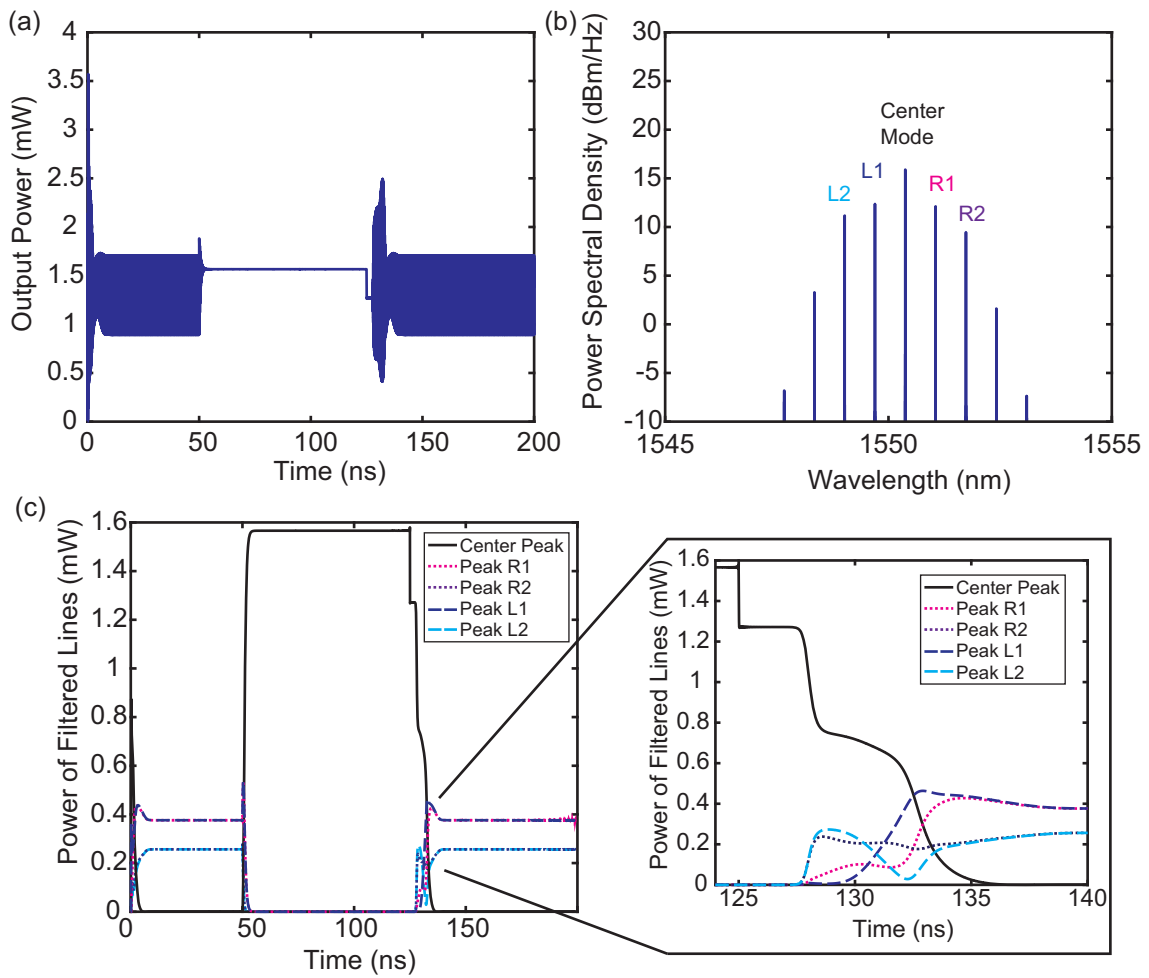FIG. 5. Simulated results of turning off and on the population grating equation responsible for SHB. The grating is turned on for $t < 50$ ns, but turned off for 50 ns $< t <$ 125 ns, and turned back on for $t >$ 125 ns. (a) Temporal output of the calculated laser, showing multimode lasing before 50 ns, then single-mode lasing until 125 ns, and multimode lasing once more after 125 ns. (b) Spectrum of the output for $0 < t < 200$ ns. It is labeled to identify each mode. (c) Modal envelopes after filtering the spectrum in (b), with labels corresponding to each mode, with an inset at 125 ns.

lengths are

$$\tau_{\text{cw,GaAs}} = 11 \, \text{ps}, \quad \tau_{\text{cw,InGaAsP}} = 5.8 \, \text{ps},$$

$$L_{D,\text{GaAs}} = 149 \, \text{nm} > \frac{\lambda_{\text{GaAs}}}{2n_0} = 118 \, \text{nm},$$

$$L_{D,\text{InGaAsP}} = 64.8 \, \text{nm} < \frac{\lambda_{\text{InGaAsP}}}{2n_0} = 221 \, \text{nm},$$

thus GaAs has a significantly longer diffusion length, which essentially washes out any half-wavelength spatial grating that exists. However, in the case of InGaAsP, the diffusion length is much shorter, only about a quarter of the half wavelength. Thus in InGaAsP QW devices operating at 1550 nm, multimode generation should be possible, arising from SHB effects. By using the comparison of the diffusion length to the intracavity wavelength, we can establish a minimum recommended wavelength based upon the material, $\lambda > 2n_0 L_D$, for strong multimode lasing based on SHB. This can also be related back to τ_g as a heuristic for a minimum SHB gain g_3. To summarize the important material parameters, low carrier diffusion in the laser diode material and long operating wavelengths both significantly benefit the strength of SHB, while strong intracavity power will improve FWM effects and the coherence between modes.

To further isolate the effects of SHB, we solve Eqs. (1) and (2) for the InGaAsP parameters but we then turn the grating term off for 50 ns $< t <$ 125 ns, and then turn it on again for $t >$ 125 ns. In Fig. 5(a), we see the dynamics play out in time: The output reaches a phase-locked state until 50 ns, when it abruptly simplifies to a single mode due to the absence of SHB, and then resumes multimode lasing after 125 ns when SHB is turned back on. We can track the individual mode envelopes [as labeled in Fig. 5(b)] by applying a simple spectral filter to each comb line in frequency domain and inverse Fourier transforming the central group of modes back into time domain. Figure 5(c) shows the results of the filtering and inverse transform. We see more clearly that, once SHB is turned off, all other modes decay rapidly until only the center mode remains. When SHB is turned back on, the central mode immediately drops in power due to increased self-saturation,

while simultaneously the sideband amplitudes start increasing from reduced gain competition. When the central mode is strong, our perturbative analysis is most accurate, as it predicts the decay of the sidebands in the absence of SHB and growth in the presence of SHB as seen in the numerical results. Eventually the sidebands become strong enough to saturate the central mode's gain and all modes mix together, reaching the same phase-locked state as before [Fig. 5(c)]. The dynamics of the individual modes are consistent with our previous analytic results, which show that the sidebands grow primarily due to increased available gain due to increased self-saturation of the central mode. We note that while the center mode emerges as the strongest mode when SHB is turned off, it is rather weak in the phase-locked solution. The phase-locked spectral shape [Fig. 3(b)] is nearly identical to that in radio-frequency FM signals for moderately strong modulation.

V. CONCLUSION

We have explained in detail the physics behind the generation of FM combs in QW diode lasers. Spatial hole burning allows multiple modes to achieve threshold gain due to reduced gain competition between modes, and the four-wave mixing induced by population pulsations locks the phases of the modes together. While SHB is easily achieved in QD lasers and QCLs, proper selection of materials can also allow SHB to exist in QW systems. With the presence of both SHB and FWM, a FM comb emerges passively as a natural state of operation of these diode lasers. This understanding should open up the possibilities of using QW diode lasers as a simple, yet effective, device for chip-scale frequency-comb applications.

[1] S. T. Cundiff and J. Ye, Rev. Mod. Phys. **75**, 325 (2003).

[2] T. Udem, J. Reichert, R. Holzwarth, and T. W. Hansch, Phys. Rev. Lett. **82**, 3568 (1999).

[3] I. Coddington, W. C. Swann, and N. R. Newbury, Phys. Rev. Lett. **100**, 013902 (2008).

[4] S. A. Diddams, T. Udem, J. C. Bergquist, E. A. Curtis, R. E. Drullinger, L. Hollberg, W. M. Itano, W. D. Lee, C. W. Oates, K. R. Vogel, and D. J. Wineland, Science **293**, 825 (2001).

[5] P. J. Delfyett, L. T. Florez, N. Stoffel, T. Gmitter, N. C. Andreadakis, Y. Silberberg, and J. P. Heritage, IEEE J. Quantum Electron. **28**, 2203 (1992).

[6] C. Calo, V. Vujicic, R. Watts, C. Browning, K. Merghem, V. Panapakkam, F. Lelarge, A. Martinez, B. E. Benkelfat, A. Ramdane, and L. P. Barry, Opt. Express **23**, 26442 (2015).

[7] K. Sato, IEEE J. Sel. Topics Quantum Electron. **9**, 1288 (2003).

[8] R. Rosales, K. Merghem, C. Calo, G. Bouwmans, I. Krestnikov, A. Martinez, and A. Ramdane, App. Phys. Lett. **101**, 221113 (2012).

[9] R. Rosales, S. G. Murdoch, R. Watts, K. Merghem, A. Martinez, F. Lelarge, A. Accard, L. P. Barry, and A. Ramdane, Opt. Express **20**, 8649 (2012).

[10] A. Hugi, G. Villares, S. Blaser, H. C. Liu, and J. Faist, Nature (London) **492**, 229 (2012).

[11] M. Gioannini, P. Bardella, and I. Montrosset, IEEE J. Sel. Topics Quantum Electron. **21**, 1900811 (2015).

[12] J. B. Khurgin, Y. Dikmelik, A. Hugi, and J. Faist, App. Phys. Lett. **104**, 081118 (2014).

[13] P. Bardella, L. L. Columbo, and M. Gioannini, Opt. Express **25**, 26234 (2017).

[14] Z. Lu, J. Liu, P. Poole, Z. Jiao, P. Barrios, D. Poitras, J. Caballero, and X. Zhang, Opt. Commun. **284**, 2323 (2011).

[15] Z. Jiao, R. Zhang, X. Zhang, J. Liu, and Z. Lu, IEEE J. Quantum Elecron. **49**, 1008 (2013).

[16] J. Faist, G. Villares, G. Scalari, M. Rösch, C. Bonzon, A. Hugi, and M. Beck, Nanophotonics **5**, 272 (2016).

[17] G. P. Agrawal, J. Opt. Soc. Am. B **5**, 147 (1988).

[18] A. Mecozzi, Opt. Lett. **19**, 640 (1994).

[19] A. Godard, G. Pauliat, G. Roosen, and E. Ducloux, IEEE J. Quantum Electron. **40**, 970 (2004).

[20] H. Rieck, Solid State Electron. **8**, 83 (1964).

[21] R. Nietzke, P. Panknin, W. Elsäßer, and E. O. Göbel, IEEE J. Quantum Electron. **25**, 1399 (1989).

[22] S. Diez, C. Schmidt, R. Ludwig, H. G. Weber, K. Obermann, S. Kindt, I. Koltchanov, and K. Petermann, IEEE J. Sel. Topics Quantum Electron. **3**, 1131 (1997).

[23] P. P. Baveja, D. N. Maywar, and G. P. Agrawal, IEEE J. Sel. Topics Quantum Electron. **18**, 899 (2012).

[24] J. Renaudier, G.-H. Duan, P. Landais, and P. Gallion, IEEE J. Quantum Electron. **43**, 147 (2007).

[25] D. J. Jones, L. M. Zhang, J. E. Carroll, and D. D. Marcenac, IEEE J. Quantum Electron. **31**, 1051 (1995).

[26] M. Homar, S. Balle, and M. S. Miguel, Opt. Commun. **131**, 380 (1996).

[27] W. W. Chow, S. W. Koch, and M. S. Sargent III, *Semiconductor-Laser Physics* (Springer-Verlag, Berlin, 1994).

[28] M. Dong, N. M. Mangan, J. N. Kutz, S. T. Cundiff, and H. G. Winful, IEEE J. Quantum Electron. **53**, 2500311 (2017).

[29] J. R. Ackerhalt, Phys. Rev. Lett. **46**, 922 (1981).

[30] T. Herr, K. Hartinger, J. Riemensberger, C. Y. Wang, E. Gavartin, R. Holzwarth, M. L. Gorodetsky, and T. J. Kippenberg, Nat. Photonics **6**, 480 (2012).

[31] L. F. Tiemeijer, P. I. Kuindersma, P. J. A. Thijs, and G. L. J. Rikken, IEEE J. Quantum Electron. **25**, 1385 (1989).